Kinetic Investigation of a Mechanism for Generating Microstructures on Polycrystalline Substrates Using an Electroplating Process

T. A. Soares[*1,2], H. Mozaffari[2], H. Reinecke[1]
[1]Universität Freiburg - IMTEK, [2]Hochschule Furtwangen (Campus Tuttlingen)
* Kronenstraße 16 . 78532 Tuttlingen, Germany, tiago.soares@saturn.uni-freiburg.de

Abstract: The purpose of this study is to understand the growth mechanism of copper (Cu) films on a Cu-Zn system substrate with a pre-defined pattern. The pattern was defined by conducting a selective etching process on a two-phase polycrystalline substrate. Because of the differences in the chemical potentials of the crystal phases, the etching rate between the alpha and beta crystals were also different. As a result of this process, there were etched regions correspondent to beta-phase crystals and quasi non-etched regions that belong to alpha-phase crystals. Afterwards, the entire surface was covered with a polymer coat, and after drying, a polishing process was conducted in order to develop the pre-defined pattern, consisting of conductive and electrically insulated regions, which are confined to the crystal dimensions. Finally, microstructure patterns were generated through electrodeposition.

Keywords: Electrodeposition, polycrystals, heterogeneous solutions, microstructures, COMSOL.

1. Introduction

In the present work, micro-fabrication of Cu structures was performed by means of electrodeposition on heterogeneous polycrystalline substrate (α+ β) crystals. The width of the generated microstructures was basically defined by the size of the substrate's crystalline grains. Usually, these dimensions range from few µm to 100 µm. In accordance with the adopted strategy, part of the grains had their surface protected with an insulate film, while the unprotected areas acted as regions of nucleation and/or growth of Cu films.

Due to the non-uniform electric field and corner effects, the observed growth tends to be faster in certain regions than others [1], [2]. This effect brings limitations on the height of the created pattern. In other words, after several seconds of deposition, the generated patterns start to narrow their cavities, until closing the entire plated surface, and forming a homogenous region [3], (Figure 1).

Considering the above mentioned phenomenon, a numerical model based on Faraday´s law in differential form was elaborated [4]. Butler-Volmer relations were also considered as boundary conditions for the anode and cathode reactions. 2D and 3D numerical models were solved by using a finite elements method with the software COMSOL.

The generated microstructures on commercial metal polycrystalline substrates can change the physical-chemical properties of the surface in many different alloys.

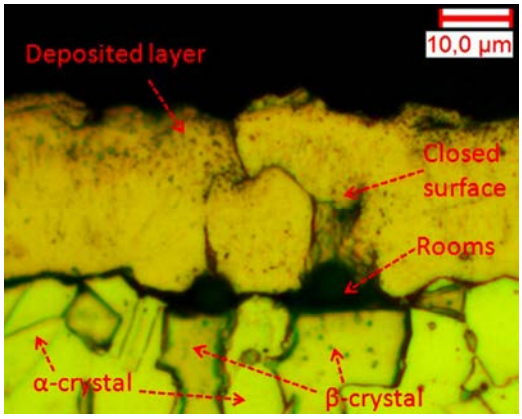

Figure 1. Closed surface due to the non-uniform electric field and corner effects

2. Fabrication Process

Basically, the developed process consists of three simple steps: 1. Etching, 2. Patterning and 3. Deposition.

2.1 Etching

Most of industrial alloys are composed of polycrystalline structures. These structures are a group of crystalline grains, with different shapes and atomic orientations. Depending on the composition of these solid materials, it is possible to have two or more phases in

thermodynamic equilibrium, and this is called a heterogeneous solution. In the present work, a $CuZn_{37}$ system is used as an electrode material. At this composition (37% Zn and 63% Cu), two phases (α+β), or a mixture of two crystal structures (FCC - Face-centered cubic and BCC - Body-centered cubic) can be in equilibrium (Figure 3.). By using Gibbs' free energy composition curves as function of the temperature, the phase boundaries of the studied system can be represented by the following diagram (Figure 2.), [6].

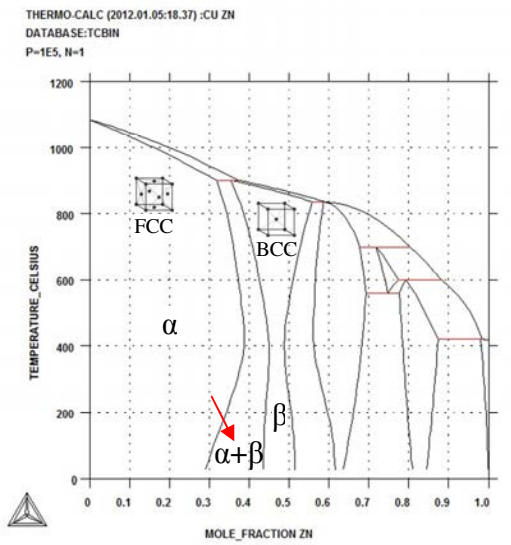

Figure 2. Calculated phase diagram of the CuZn system

Since the mentioned system is in equilibrium, the energy level of both phases is the same. However, looking at the surface, the difference between crystal structures and composition can considerably change the surface energy of one phase, in comparison to the other. In other words, the number of free bonds of atoms on the crystal surface, and the enthalpy of interaction between atoms ($H_{Cu\text{-}Zn}$ $H_{Cu\text{-}Cu}$, $H_{Zn\text{-}Zn}$) are different [7]. As to the composition of the phases, it can be calculated through the "lever rule": $X_{Zn}^{\alpha} \approx 33\%$, $X_{Zn}^{\beta} \approx 44\%$. Then, if the concentration of Zinc is higher on the β phase, the chance of dezincification in an acid solution can be higher. Additionally, due to the difference in corrosion potentials, and $\Delta G_{(surface)}^{\alpha\text{-}\beta} < 0$ [9], a local redox reaction can occur spontaneously along the crystal phases, in which the β phase would work as an anode.

Considering the points above, a solution of 50 ml HNO_3 65% and 50 ml of distillated water was prepared [9]. The result of the etching process is depicted at (Figure 4).

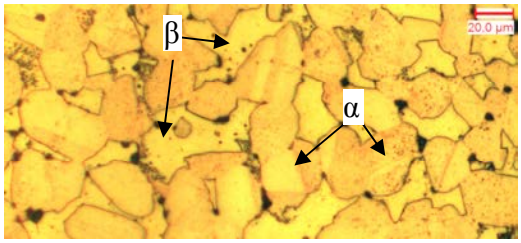

Figure 3. Micrographic picture of $CuZn_{37}$ (α+β phases)

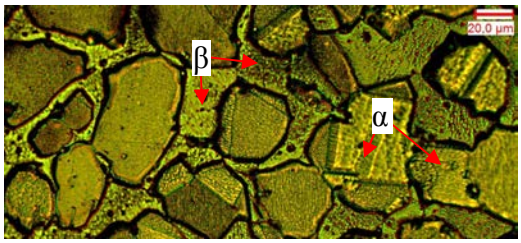

Figure 4. After conducting a selective etching process, the etching rate of β-phase was higher than the rate on α-phase

2.2 Patterning

In sequence, the whole sample was covered with a mixture of resin and solvent and left to dry for two minutes in standard conditions. Afterwards, polishing process (3 µm) was conducted during 1 min in order to remove the polymer layer. As a result, there were isolated regions above the β-crystals and metal regions which belong to the α-crystals. Figure 5 demonstrates the result of this step.

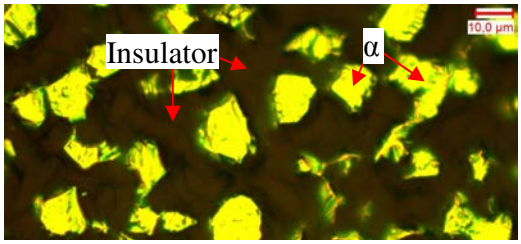

Figure 5. Results of the patterning phase

Although the presented patterning process can be perceived as simple, more sophisticated

techniques, such as spin coating, could be used to increase precision in filling the etched regions.

2.3 Deposition

Subsequently, electrodeposition was conducted in a standard $CuSo_4$ electrolyte. A hot stirring plate was used in order to reasonably keep a constant temperature and a uniform agitation in the bath. The voltage was kept in 400 mV, and the plating time was up to 410s. The sequence of plating can be followed in Figure 7.

a. Deposition time: 0-10s **b.** Dep. time: 10-110s

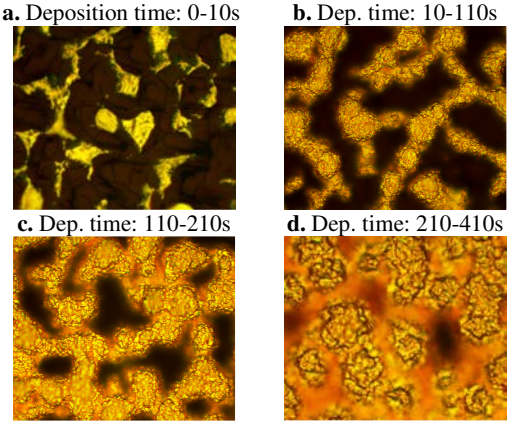

c. Dep. time: 110-210s **d.** Dep. time: 210-410s

Figure 6. Progress of the deposition **(a, b c, d)**

As shown in the figure above, with the developed method, it was possible to generate microstructures through a polycrystalline surface. However, as expected [3], after approximately 200s (picture c), the structures start to narrow their cavities until sealing the entire surface (picture d). This effect can be explained due to the high concentration of the electric field on the corners of the growing structures. Thereby, the deposition rate at these regions can be higher than on the others in the middle of the "grain". In the next section, the dynamic of this process will be explored. Furthermore, a relationship between deposition time, width of the seed grain and the maximum possible rate will be set by simulations (Section 4).

3. Kinetic theory and basic equations

In the previous section, thermodynamic concepts were briefly introduced, in an effort to predict the spontaneity of a reaction. On the other hand, it is also important to emphasize that the evolution of mass-flows throughout the system is determined by electrochemical kinetics. From Maxwell Boltzmann distribution, Transition State Theory, Van´t Hoff, Arrhenius and Eyring equation, it is possible to describe the main relations between the activation energy, the equilibrium and rate constants, as well as temperature and a frequency factor. Subsequently, from the Nernst and Tafel plots, the Butter-Volmer model could finally be obtained, and hence, valuable information about electrochemical experiments could be provided. Equation 1 shows the Butter-Volmer model that will later be used as the boundary conditions for the cathode and anode during the simulations:

I.
$$i = i_0\left[\frac{C_o(0,t)}{C_o^*}e^{-\alpha\cdot f\cdot\eta} - \frac{C_R(0,t)}{C_R^*}e^{(1-\alpha)\cdot f\cdot\eta}\right]$$

Where,

- i = Input current
- i_0 = Equilibrium current (when the cathodic and anodic current are the same: $i_{anodic} = i_{cathodic} = i_0$)
- α = transfer coefficient (position of the activation complex within the span of the reaction)
- η = Over potential ($\eta = E - E_{eq}$)
- f = F/RT (Faraday constant relations)
- C_o = Concentration of the oxidant species close to the electrode
- C_R = Concentration of the reductant species close do the electrode
- C_o^* = Concentration of the oxidant species in the bulk solution
- C_R^* = Concentration of the reductant species in thebulk solution

And for the insulate regions, equation II is applied.

II.
$$i = 0$$

Continuing with the modeling of the electrical chemical cell, it is possible to demonstrate a direct proportionality between the faradic current and the electrolysis rate (N) [2]:

III.
$$I = \frac{dQ}{dt}(columbs/s)$$

IV.
$$\frac{Q}{nF} = N$$

Then, by III and IV, the rate of the reaction can be computed as follows:

V. $$\frac{dN}{dt} = \frac{i}{n \cdot F}$$

Where "n" is the stoichiometric number of the reaction. Since the electrode reactions are heterogeneous and occur only at the interface, the rate of the reaction strongly depends on the mass transfer to the electrode and several surface effects. Therefore, the rate as function of the area is applied:

VI. $$\frac{N}{dt}\left(\frac{mol}{s \cdot m^2}\right) = \frac{i}{nFA} = \frac{J}{nF}$$

Where, J is the current density.
In view of the net rate of the electrode reaction, it can be inferred that it is conditioned by the rate in which electroactive species are brought to the double layer [2]. Therefore, the current density can be expressed in terms of mass transfer, by following the Nernst-Planck relations (in one dimension):

VII. $$J_i(x) = -D_i \cdot \frac{\partial C_i(x)}{\partial x} - \frac{z_i F}{RT} \cdot D_i \cdot C_i \cdot \frac{\partial \phi(x)}{\partial x} + C_i \cdot \upsilon(x)$$

Where, the first term of this partial differential equation represents the mass transfer by diffusion, the second term being the mass transfer migration and last term being the mass transfer by convection (which will be neglected on the simulations). And:

x	=	Distance from the surface (m)
D_j	=	Diffusion coefficient of the species i (m^2/s)
z_i	=	Charge (dimensionless)
C_i	=	Concentration of the specie i (mol/m^3)
ϕ	=	Electric potential
$\upsilon(x)$	=	Velocity of a volume element in the solution along the x direction (m/s)

Thus, by solving the Nernst-Planck equation in combination with equation VI, it is possible to obtain an overview, with a considerate level of precision, about the dynamics of the growth of the generated microstructures in one dimension.

For solving this differential equation (VII), equations I and II are used as boundary conditions. It is also important to mention that the conservation of the matter in an electrode reaction must be respected, therefore:

VIII. $$J_O(0,t) = -J_R(0,t) \text{ and;}$$

IX. $$D_o\left[\frac{\partial C_O(x,t)}{\partial x}\right]_{x=0} + D_R\left[\frac{\partial C_R(x,t)}{\partial x}\right]_{x=0} = 0$$

Moreover, by using a vector form, expressed in equation XX, the Nernst-Planck equations can be expanded in two or more dimensions.

X. $$j_i(r) = -D_i \cdot \nabla \cdot C_i(r) - \frac{z_i F}{RT} \cdot D_i \cdot C_i \cdot \nabla \cdot \phi(r) + C_i \cdot \upsilon(r)$$

4. Use of COMSOL Multiphysics

In this section, the software COMSOL was used in order to solve the partial differential equation previously presented. The software is based on the Finite Element Methods (FEM) and can be applied to solve numerically transient problems. One of the main assets of the software is the possibility of visualizing the process of deposition, which is simulated by the movement of the generated mesh (small elements that can be solved in relation to each other).

4.1 Calibration of the generated model

As a first step, a 2D model was calibrated based on the results of Figure 6 (b). The simulations' results were adjusted in order to achieve microstructures of 10μm at 210s with a difference in potential in a cell of 400mV. The calibrated variables are presented in Table 1 and at Figure 7.

Table 1: Calibrated variables

C_{init}	=	200 mol/m^3	Initial concentration (Initial condition)
T_0	=	303 K	Temperature of the experiment
V	=	400 mV	Applied voltage
α	=	1,4	Transfer coefficient
D_i	=	$1{,}75 \times 10^{-9}$	Diffusion coefficient for all species

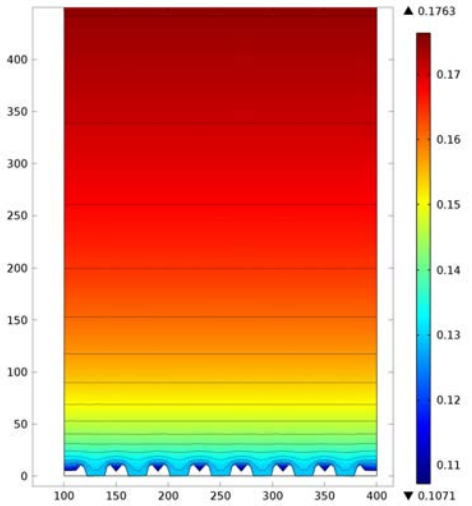

Figure 7. Generated and calibrated model by FEM (the gradient scale represents the distribution of the electrolyte potential. This scale is the same for the next simulated pictures)

4.2 2D Simulations

As a next step, the maximum possible growth, without sealing the entire surface, was calculated as function of the supposed width of the crystals. Values of 5µm, 10µm, 20µm and 50µm were chosen. Figure 8 to Figure 11 depict the results.

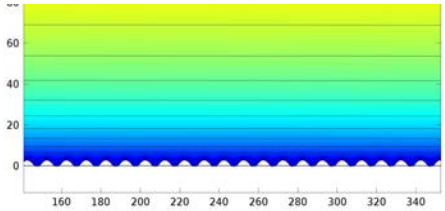

Figure 8. Crystal width: 5µm

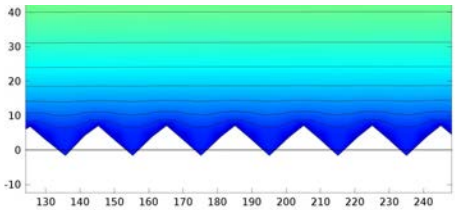

Figure 9. Crystal width: 10µm

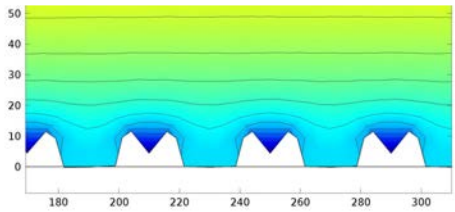

Figure 10 Crystal width: 20µm

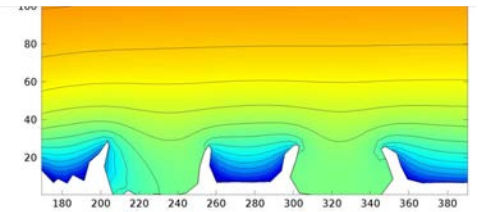

Figure 11. Crystal width: 50µm

5. Results and discussion

As a result of the simulation, it was possible to establish a relationship between the grains' sizes, the maximum possible height and the maximum deposition time of the generated microstructure. Graph 1 shows this interaction:

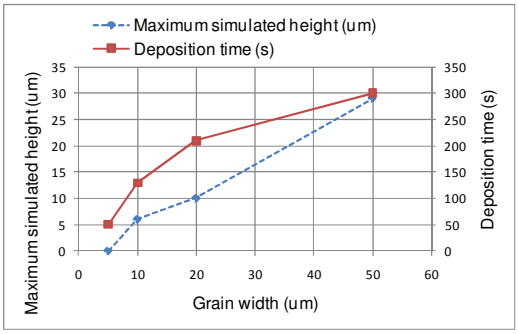

Graph 1. The grains' sizes as function of the maximum height and the deposition time

Due to the limitations of the software, it is not possible to continue with the simulation when the cavities start to close. At this point, the elements of the moving meshes are so close to one other that the algorithms do not converge to a result and the system is unable to continue. However, since the aim is to have the maximum possible growth without sealing the cavities, the maximum deposited time was considered when the system interrupts the simulation.

Thus, as expected, with the increase of the grain´s size, it was possible to achieve higher microstructures. For instance, for a value of grain

width of 20µm, the microstructures have dimensions (maximum height) up to app. 10µm in app. 210s. These results are based on numerical simulations. Surfaces' effects, such as dislocations, that could change the deposition rate and the dynamic of the process, are not taken into account. As demonstrated, the idea is just to show that in perfect situations, the electric field has a great impact in the process of deposition and growth.

5.1 3D Simulation

In order to exemplify the deposition in 3 dimensions, the following model was created. The figures below (Figures 12 and 13) show the results of the simulation in real polycrystal.

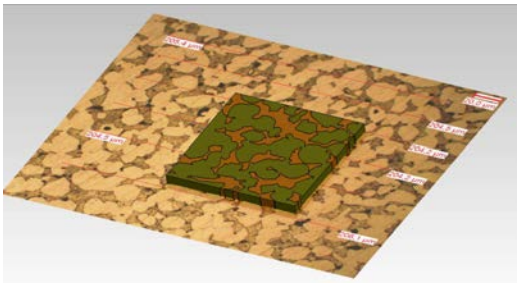

Figure 12. Micrographic modeling of a $CuZn_{37}$ crystal structure (Grain's size: app. 22µm)

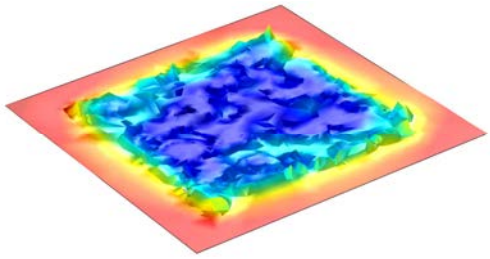

Figure 13. 3D simulation of the maximum growth of the α phase – maximum achieved height: 12.3µm

6. Conclusions

In this work, finite elements methods were conducted in order to evaluate the kinetic of the growth of microstructures using electrodeposition. According to the adopted process, the height of the microstructures could be modeled by adjusting the size of the cathode crystal grains, e.g. conducting a pre-heat treatment, prior to the process, and by the plating time. It was observed that the maximum possible height without sealing of the cavities is of about half of the width of the grain size.
The developed microstructures can change the physical-chemical properties of their surfaces in many different alloys. Biocompatibility of implants' parts [5], anti-bacterial and catalytic functions of the surface could be enhanced by conducting the presented process.

7. References

1. N. Kanani, Electroplating Basic Principles, Process and Practice, First Edition, Oxford - UK, Elsevier, 2004, ISBN 1856174514
2. Allen J. Bard, Larry R. Faulkner. Electrochemical Methods: Fundamentals and Applications. Austin, Texas: John Wiley & Sons, Inc, 2001, ISBN 0-471-04372-9.
3. N. G. Sarius et. al, Electroplating of Nickel in Grooves Under the Influence of Low and Medium Frequency Ultrasound, *Journal for Electrochemistry and Plating Technology*, **1**, 19 28, (2011)
4. J. Deconinck, Mathematical modeling of electrode growth, *Journal of Applied Electrochemistry*, **24**, 212-218, (1994)
5. Charest, Joseph L. Topographic and chemical patterning of cell surface interfaces to influence cellular. PhD Dissertation - Georgia Institute of Technology (2007)
6. TC Binary Solutions Database (v1.0, 2006), Thermo-Calc Software AB, Stockholm, Sweden, SGTE, Scientific Group Thermodata Europe
7. T. Nishizawa, Thermodynamics of Microstructures, USA, ASM International, 2008, ISBN-13: 978-0-87170-716-1
8. Petzow G., Materialkundlich-Technische Reihe 1 – Metalographisches Ätzen, 5th Edition, Stuttgart - DE, Gebrüder Borntraeger, 1976, ISBN 3-443-230016
9. Nestor Perez, Electrochemistry and Corrosion Science, New York USA, Kluwer Academic Publishers, 2004, ISBN 1-4020-7744-0

8. Acknowledgements

Hochschule Furtwangen (Campus Tuttlingen), Kooperatives Promotionskolleg Generierungsmechanismen für Mikrostrukturen "GenMik", LGFG, Universität Freiburg.